RSC Advances

ROYAL SOCIETY OF CHEMISTRY

www.rsc.org/advances

1   *In situ* synthesis of gold nanoparticles on LBL coated nanofibers by tannic acid

2   for catalytic application

3   Bin Zhou[a,b], Xing Jin[c],Hongshan Liang [a,b], Jing Li [a,b], Shilin Liu[a,b], Yan Li[a,b], Yijie

4   Chen[a,b], Bin Li[a,b]*

5   [a] College of Food Science and technology, Huazhong Agriculture University,

6   Wuhan 430070, China,

7   [b] Key Laboratory of Environment Correlative Dietology (Huazhong Agricultural

8   University), Ministry of Education

9   [c] Department of Clinical Laboratory, Xi'an Gaoxin Hospital, Xi'an 710075,China

10   * Corresponding author: Bin Li Tel.: +86 27 6373 0040 Fax: +86 27 8728 8636

11   E-mail: libinfood@mail.hzau.edu.cn

12

13

14

15

16

17

18

19

20

21

22

Abstract:

Electrospinning nanofibrous mats are extensively studied as efficient two-dimensional nanomaterials applied in the fields of filtration, catalysis, and biosensors due to their flexibility and porosity. In this article, gold nanoparticles (AuNPs) loading composite nanofibers were fabricated by a simple method, which consisted of the preparation of the nanofibers by electrospinning, the deposition of tannic acid (TA) on the surface of the nanofibers via layer-by-layer assembly and the reduction of the AuNPs on the nanofibrous mats. The as-prepared nanofibers were characterized by scanning electron microscopy (SEM), energy dispersive spectroscopy (EDS), transmission electron microscopy (TEM), Fourier transform infrared spectroscopy (FTIR), X-ray diffraction (XRD), and X-ray photoelectron spectroscopy (XPS), respectively. The results revealed that AuNPs successfully generated on the nanofibers without aggregation. In addition, by adjusting the number of the bilayer in the assembly process, the content of gold supported on the nanofibrous mats could be easily controlled. The catalytic performance of the hybrid nanofibrous mats to the reduction of 4-nitrophenol (4-NP) with sodium borohydride were monitored by UV–visible spectroscopy (UV-vis). Notably, the hybrid composite nanofibrous mats could be easily separated from reaction mixture.

Keywords: Electrospinning, Layer-by-layer, Tannin acid, gold nanoparticles, Catalysis

1. Introduction

During the past decade, noble metallic nanoparticles, such as Au, Ag, Pt, have received considerable interest due to their unique physical and chemical properties and their potential utility in catalysis, such as the reduction of 4-nitrophenol (4-NP) to 4-aminophenol (4-AP) [1, 2], CO oxidation [3], propylene epoxidation [4], and the oxidation of alcohols [5, 6].

As is well-known, 4-NP is a common organic pollutant in industrial and agricultural waste water [7]. In recent years, the reduction of 4-NP in the presence of sodium borohydride ($NaBH_4$) has been extensively studied for the efficient and eco-friendly production of 4-AP, which is a vital intermediate for the manufacture of analgesic, antipyretic drugs, corrosion inhibitor [8, 9]. To make the route possible, various noble metals, including Au, Ag, Pt nanocrystals and alloys have been widely used due to their outstanding catalytic activities [8, 10, 11].

However, smaller unsupported nanoparticles tend to easily aggregate owing to their large surface area-to-volume ratio and are difficult to remove from the reaction media [8]. Thus, we ought to discover an alternative method or material which remains merits and overcomes disadvantages of the materials. To overcome these limitations, the immobilization of nanoparticles on suitable substrate was an alternative way.

Recently, the impact of membrane technology has exponentially increased in research settings and industrial applications [12]. Two dimensional membrane

67　materials that are constructed by micro- or nano-fibers are intensively applied

68　as substrate materials in the fabrication of functional nanomaterials due to their

69　flexibilities, high specific surface area and porosity [13].

70　Electrospinning is an attractive way for manufacturing nanofibers with

71　controllable compositions and structures[14]. It is an efficient and straightforward

72　method of producing ultrafine fibers with micro- to nano-scale and with

73　controlled surface morphology. Electrospun nanofibrous membranes possess

74　several attractive features, such as large surface-to-volume ratio, high porosity,

75　and interconnected open pore structure [15], which make them very attractive in

76　separation technology and catalysis, et al.

77　The combination of nanoparticles into electrospun nanofibers has been

78　performed predominately using two different ways. One method is the *in situ*

79　generation of particles in the fiber support by co-electrospinning a mixed

80　solution of polymer and desired metal salt. Subsequent heating of the

81　membrane yields fibers decorated with metal nanoparticles in both the interior

82　and exterior of the fiber. An alternative is the post-treatment of the membrane

83　in order to deposit metal nanoparticles strictly on the surface of the fibers.

84　In this current work, freshly prepared electrospun cellulose nanofibrous

85　membranes were first coated with lysozyme (Lys) and tannic acid (TA) via

86　layer-by-layer assembly technique. Then, AuNPs were *in situ* reduced by TA

87　and immobilized into the Lys/TA shell. Scanning electron microscopy (SEM),

88　Fourier transform infrared (FTIR) spectroscopy, transmission electron

89 microscopy (TEM), energy dispersive spectroscopy (EDS), X-ray diffraction

90 (XRD), and X-ray photoelectron spectroscopy (XPS) were utilized to

91 characterize the morphology and composition of AuNPs-containing

92 nanofibrous membranes. Finally, the catalytic properties of

93 AuNPs-immobilized composite nanofibers were investigated using 4-NP as a

94 model substrate. The results revealed that the composite nanofibrous

95 membranes displayed fine catalytic efficiency to reduce 4-NP to 4-AP.

96 **2. Materials and methods**

97 **Materials**

98 Cellulose acetate (CA, *Mn* 30,000) was purchased from Sigma–Aldrich Co.,

99 USA. Hen egg white lysozyme, $HAuCl_4 \cdot 3H_2O$, sodium borohydride ($NaBH_4$)

100 and 4-nitrophenol (4-NP) were obtained from the Sinopharm Chemical

101 Reagents Co., Ltd. (Shanghai, China). Tannic acid was purchased from

102 Aladdin Chemistry Co. Ltd. (Shanghai, China). The other reagents were

103 analytical grade purchased from China National Pharmaceutical Group

104 Industry Corporation Ltd. All aqueous solutions were prepared using purified

105 water with a resistance of 18.2 MΩcm.

106 **Fabrication of template nanofibers**

107 CA nanofibers were fabricated by using modified Ding's method [16, 17]. 17% CA

108 solution was prepared by dissolving CA powder in a mixed solvent

109 (acetone/DMAc = 2:1 w/w). The homemade equipment consisted of a syringe

110 pump (LSP02-1B, Baoding Longer Precision Pump Co., Ltd., China) and a

111   high voltage power supply (DW-P303-1ACD8, Tianjin Dongwen Co., China). A

112   grounded cylindrical layer was used as a collector which rotated with a

113   rotational velocity of 50rpm. The applied voltage was 17 kV and the

114   tip-to-collector distance was 20 cm. The ambient temperature and relative

115   humidity was maintained at 25℃ and 45%, respectively. The prepared mats

116   were dried at 40 ℃ in vacuum for 24 h to remove the trace solvent. The CA

117   mats were hydrolyzed in NaOH solution (0.05M) at room temperature for 7

118   days following the previous reports [18, 19].

119   **Construction of nanocomposite membranes on cellulose nanofibers**

120   The bilayer film was then deposited, by spraying Lys (1 mg/mL lysozyme, pH

121   7.4, in 0.01 M PBS) followed by tannic acid (1 mg/mL, pH 7.4, in 0.01 M PBS)

122   each for 10mL solution. After each deposition step, a 5 second wash with 0.01

123   M PBS (pH 7.4) was sprayed [20, 21]. Here, $(Lys/TA)_n$ was used as a formula to

124   label the LBL structured films, where n was the number of the Lys/TA bilayers.

125   The LBL films coated fibrous mats were dried at 40 ℃ for 2 h under vacuum

126   prior to further characterizations .

127   **Characterization of composite nanofibrous membranes**

128   The surface morphologies and chemical compositions of the composite

129   nanofibrous mats were measured by scanning electron microscopy (SEM) and

130   energy dispersive spectroscopy (EDS) with a JEOL JSM-6390LV SEM

131   equipped with an Oxford INCA EDS detector. Fourier transform infrared (FT-IR)

132   spectra were acquired on a Nicolet170-SX instrument (Thermo Nicolet Ltd.,

133 USA) in the wavenumber range of 4000-400 cm^{-1}. The cross-sections of the

134 nanofibers were observed using a JEOL transmission electron microscope

135 (H-7650, Hitachi, Japan). X-ray photoelectron spectroscopy (XPS) was

136 conducted on an axis ultra DLD apparatus (Kratos, U.K.). X-ray diffraction

137 (XRD) was carried out using a diffract meter type D/max-rA (Rigaku Co.,

138 Japan) with Cu target and Ka radiation (λ= 0.154 nm).

Fabrication of AuNPs@Lys/TA composite membranes

140 The as-prepared Lys/TA composite membranes were immersed into

141 chloroauric acid solution with different concentrations (1mM and 5mM) until

142 the color of the membranes changed into dark violet. Then, they were

143 washed thoroughly with ultrapure water to remove the AuCl^{-}. Finally, the

144 AuNPs@Lys/TA composite membranes were dried at room temperature for 2

145 h under vacuum prior to further characterizations.

Catalytic reduction of 4-NP

147 To study the catalytic activity, 3 mg AuNPs@Lys/TA composite nanofibers

148 were added into 4 mL of 4-NP aqueous solution (0.12 mM). Subsequently, the

149 above solution was mixed with 4 mL fresh NaBH$_4$ solution (5 mM). The

150 reaction was carried out at 298 K with continuous stirring. Parts of the mixture

151 were filtered through a 0.22 μm membrane filter after every 2 min for the

152 determination with UV-vis absorption spectra [22].

3 Results and discussion

Surface morphology analysis of Lys/TA nanofibrous membranes

155 To investigate the impact of Lys and TA deposition on the morphology of the

156 cellulose nanofibrous membranes, the surface morphology analysis of the

157 composite fibrous mats were conducted by SEM. The representative SEM

158 images of cellulose nanofibrous mats showed in Fig. 1 revealed randomly

159 oriented 3D nonwoven mats with an average diameter of 477.3 nm. They

160 possessed loosely packed cylindrical fibers and were continuous and long

161 without any defects (Fig. 1a and a'). To study the impact of assembly process

162 and the number of coating bilayers on the formation of composite films, the

163 cellulose fibers were coated with various bilayers of Lys and TA.

164 From the SEM images, we can see that not only the diameter but also the

165 morphology of all samples changed obviously attributed to the deposited of

166 Lys and TA on the surface of nanofibers. After the LBL films were coated, the

167 nanofibers showed a higher surface roughness on each fiber compared with

168 the smooth surface of the cellulose nanofibers (Fig. 2a–d and a'–d'). As

169 revealed in Fig. 1b', c' and d', we can see that, after the assembly process, a

170 Lys/TA shell layer were visible around the cellulose nanofibers. Also, the

171 thickness of the shell layer increased with the increase of the bilayer number,

172 which led to the increase of the fibers diameter（shown in the right column of

173 Figure 1）. Mentionablely, vacuum-assisted method was used in order to keep

174 the incompact stacking style of the fibers. These images visually demonstrated

175 that Lys and TA were successfully assembled onto the surface of the cellulose

176 fibers.

FT-IR spectra of Lys/TA nanofibrous mats

Figure 2 displayed the FTIR spectra of the raw materials and the composite nanofibrous membranes. All membranes showed a abroad absorption band at about 3500~3100 cm^{-1}, which denoted the free O-H stretching vibration of hydroxyl groups [23]. Moreover, cellulose nanofibrous mats also displayed absorption bands at 1637, 1066, 1238, 1164 ,1052 and 897 cm^{-1}, corresponding to –OH bending [24], C-O sretching, C-O-C asymmetric stretching and C$_1$-H deformation vibrations, respectively [25] (figure 2e). The spectrum of Lys, showed in figure 2a, contained two characteristic peaks. The amide I band (about 1654cm^{-1}) was relevant to the C=O stretching mode, whereas the amide II band (about 1540 cm^{-1}) was attributed to the stretching mode of N-H vibrations [26, 27]. For the LBL coated films, the observed increase in intensity of the absorption band at 1716 and 1615 cm^{-1} as shoulders of the amide I or –OH bending was due to the carbonyl CO vibration of the TA ester bond and C=C stretching vibrations of aromatic ring, respectively [17]. In addition, compared with the spectrum of cellulose nanofibers, the presence of the peak located at 1540 cm^{-1} and accompanied with a shoulder peak was attributed to the N-H vibrations and C=C stretching vibrations, respectively (figure 2a, b, c, and d). For the composite membranes, the enhancement of the band at 1323 cm^{-1} and 1204 cm^{-1} was caused by the C-O stretch of the acid group in TA and C-O stretch in polyols, respectively [28]. The band at 759 cm^{-1} could be related to the C-H out plane bend of phenyl group [29]. On the base of the above results, we

199 could see that Lys and TA were deposited on the surface of the cellulose

200 fibers.

201 **Surface and cross-sectional morphology analysis of AuNPs@Lys/TA**

202 **nanofibrous membranes**

203 The AuNPs were synthetized in the shell of the Lys/TA nanofibers via *in situ*

204 reduction. In order to comfirm the generation of AuNPs, the surface and

205 cross-sectional morphology analysis of AuNPs-immbolized Lys/TA

206 nanofibrous membranes was performed by SEM and TEM, respectively. The

207 SEM images of (AuNPs@Lys/TA)$_{10}$ were displayed in figure 3. Round-shaped

208 AuNPs with a relatively uniform distribution were clearly observed, illustrating

209 that AuNPs were successfully generated along the cross section of the fibers.

210 It can be seen that an obvious morphological transformation of the Lys/TA

211 nanofibers surface from relatively smooth to coarse appeared after LBL

212 assembly process.

213 We also investigated the morphology and size distribution of AuNPs in the

214 Lys/TA shell. Figure 4 displayed the cross-sectional TEM images of

215 AuNP-containing Lys/TA composite nanofibers and the size distribution

216 histogram of the AuNPs formed in the shell. Clearly, AuNPs were

217 homogeneously distributed within the Lys/TA shell, forming a nanometer-scale

218 thick composite coating around the cellulose fiber core. It can be seen that

219 almost all of the AuNPs were embedded in the Lys/TA matrix. The average

220 diameter of the AuNPs was about 20.78 nm obtained by Nano Measurer 1.2.

221   Mentionablely, we found that the size of AuNPs on the outmost layer was

222   larger than the inners' mainly caused by higher AuCl$^-$ concentration at the

223   interface. The AuNPs revealed a larger particle size of 39.52 nm, when

224   synthetized in AuCl$^-$ solution (5mM) (Figure S1).

225   **Surface composition measurement of the composite nanofibrous membranes**

226   More detailed information regarding the chemical and bonding environment of

227   the composite nanofibrous membrance ((AuNP@Lys/TA)$_{10}$) was ascertained

228   using XPS and EDS. Figure 5a showed the survey scanned spectra in the

229   range of 0-1000 eV. The overview spectra revealed that C 1s, O 1s, N 1s, S 2p,

230   and Au 4f existed in (AuNP@Lys/TA)$_{10}$, however, only C and O elements

231   existed in bare cellulose nanofibers [30]. The C 1s core-level photoelectron

232   spectrum (Figure 5b) could be curved into three peak components located at

233   about 284.6 eV, 286.4 eV, and 287.9 eV, which were attributed to C-C, C-O,

234   and C=O or O-C=O group from TA or Lys [17, 31]. Moreover, the presence of

235   peaks posited at about 400 eV and 164 eV comfimed the successfully

236   assembly of Lys and TA on the surface of the nanofibers. In addition, the Au4f

237   core-levels shows two peaks at 84.71 eV and 88.39 eV, which were assigned

238   to 4f$_{7/2}$ and 4f$_{5/2}$, respectively (Figure 5e). The position and θ difference

239   between the two peaks (3.7 eV) well matched with the value reported for Au^0,

240   suggesting the existence of Au NPs [32].

241   To further confirm the surface chemical information of the nanocomposite,

242   EDS analysis was also conducted (Figure 5f). The result disclosed the

243 elemental compositions of the nanofibrous membranes and the observed C, O,

244 N, S, and Au elements which ensured the involvement of Lys and TA in them.

245 The EDS result also confirmed the AuNPs were successfully synthetized and

246 immobilized into the nanofibers, which was consistent with the XPS results.

247 **Crystalline property of AuNPs@Lys/TA nanofibrous mats**

248 To further verify the formation of the AuNPs on the coating shell, structural

249 characterizations were conducted by XRD analysis. As shown in figure 6, XRD

250 patterns of the different samples were revealed. From figure 6a we could see

251 that cellulose nanofibers exhibited a typical cellulose II crystal with three

252 characteristic diffraction peaks at 12.2, 20.1, and 21.8° [33]. The XRD pattern of

253 the AuNPs-loading nanocomposite membranes also contained the

254 characteristic diffraction peaks of cellulose, along with 38.31°, 44.58°, 64.78°,

255 and 77.79° peaks, could be attributed to the reflections, which well matched

256 with the standard JCPDS data (040784) of *fcc* Au corresponding to the (111),

257 (200), (220), and (211) lattice planes [34, 35]. It could be seen that with the

258 increase of layer number, the diffraction peak intensity increased significantly,

259 which caused by higher amount of the AuNPs.

260 **Catalytic reduction of 4-NP**

261 We also investigated the possible application of the AuNPs-immbolized Lys/TA

262 composite nanofibers in reduction of nitroaromatic. The catalytic reduction of

263 4-NP to 4-AP with an excess amount of $NaBH_4$ become one of the model

264 reaction to evaluate the catalytic performance of novel nanoparticles [5]. The

265   colour of reaction mixture changed from light yellow to dark yellow owing to the

266   generation of 4- nitrophenolate ion with the addtion of the $NaBH_4$ [36]. As shown

267   in Figure 7a, there was little effect on the decrease in absorbance at 400 nm

268   within 24 min, indicating that neither cellulose nanofiber nor Lys/TA shell had

269   any catalytic activity for the reduction of 4-NP. Theoretically, the reaction was a

270   thermodynamically feasible process, but it was kinetically restricted in the

271   absence of a catalyst [22]. However, with the addition and proper mixing of

272   AuNPs@Lys/TA composite nanofibers, the reaction could conduct, where the

273   kinetics could be easily monitored spectrophotometrically associated with the

274   observation of a fading and ultimate bleaching of the yellow color of reaction

275   mixture.

276   The catalytic efficiency was enhanced with the increasing of the content of

277   gold on the nanofirous mats by increase the number of the bilayer.

278   Furthermore, Figure 7b showed the catalytic reaction of 4-NP over

279    $(AuNPs@Lys/TA)_5$ with high catalytic activity could be conveniently separated

280   from the reaction mixture, and would greatly promote their industrial

281   application.

282   **4 Conclusions**

283   In summary, we have successfully developed a facile and green approach to

284   synthesize and immobilize AuNPs onto cellulose nanofibers. The

285   immobilization of the AuNPs with an average diameter of 20.78 nm within the

286   Lys/TA shell did not impact the porous fibrous structure of the mats. The

287 composite nanofibrous mats were characterized by SEM, TEM, XRD, XPS,

288 and so on. Finally, the catalytic efficiency was enhanced with the increasing of

289 the number of bilayer caused by the increase of the AuNPs amount in the

290 Lys/TA shell. Notably, the AuNPs@Lys/TA composite nanofibers could be

291 easily separated from the reaction mixture.

292 **Acknowledgments**

297

298

299

300

301

302

303

304

305

306

307

308

309   **Reference**s

310   1.   B. Baruah, G. J. Gabriel, M. J. Akbashev and M. E. Booher, *Langmuir*,

311   2013, 29, 4225-4234.

312   2.   R. Ciganda, N. Li, C. Deraedt, S. Gatard, P. Zhao, L. Salmon, R.

313   Hernandez, J. Ruiz and D. Astruc, *Chem Commun (Camb)*, 2014, 50,

314   10126-10129.

315   3.   A. A. Herzing, C. J. Kiely, A. F. Carley, P. Landon and G. J. Hutchings,

316   *Science*, 2008, 321, 1331-1335.

317   4.   Y. Lei, F. Mehmood, S. Lee, J. Greeley, B. Lee, S. Seifert, R. E. Winans,

318   J. W. Elam, R. J. Meyer, P. C. Redfern, D. Teschner, R. Schlögl, M. J.

319   Pellin, L. A. Curtiss and S. Vajda, *Science*, 2010, 328, 224-228.

320   5.   J. Li, C.-y. Liu and Y. Liu, *J. Mater. Chem.*, 2012, 22, 8426.

321   6.   A. S. K. Hashmi and G. J. Hutchings, *Angew. Chem. Int. Ed.*, 2006, 45,

322   7896-7936.

323   7.   J.-R. Chiou, B.-H. Lai, K.-C. Hsu and D.-H. Chen, *J. Hazard. Mater.*,

324   2013, 248–249, 394-400.

325   8.   S. Zhang, S. Gai, F. He, S. Ding, L. Li and P. Yang, *Nanoscale*, 2014, 6,

326   11181-11188.

327   9.   Z. Zhang, C. Shao, P. Zou, P. Zhang, M. Zhang, J. Mu, Z. Guo, X. Li, C.

328   Wang and Y. Liu, *Chem Commun (Camb)*, 2011, 47, 3906-3908.

329   10.   S. Tang, S. Vongehr and X. Meng, *J. Mater. Chem.*, 2010, 20,

330   5436-5445.

331   11.   S. Zhou, K. McIlwrath, G. Jackson and B. Eichhorn, *J. Am. Chem. Soc.*,

332   2006, 128, 1780-1781.

333   12.   E. Formo, M. S. Yavuz, E. P. Lee, L. Lane and Y. Xia, *J. Mater. Chem.*,

334   2009, 19, 3878.

335   13.   J. Wang, H. B. Yao, D. He, C. L. Zhang and S. H. Yu, *ACS Appl. Mater.*

336   *Interfaces*, 2012, 4, 1963-1971.

337   14.   X. Wang, B. Ding, G. Sun, M. Wang and J. Yu, *Prog. Mater Sci.*, 2013,

338   58, 1173-1243.

339   15.   N. Wang, X. Wang, B. Ding, J. Yu and G. Sun, *J. Mater. Chem.*, 2012,

340   22, 1445-1452.

341   16.   X. Mao, B. Ding, M. Wang and Y. Yin, *Carbohydr. Polym.*, 2010, 80,

342   839-844.

343   17.   B. Zhou, J. Xing, J. Li, W. Xu, Y. Li and B. Li, *RSC Adv.*, 2014.

344   18.   J. Du, X. Li, C. Yang, W. Li, W. Huang, R. Huang, X. Zhou and H. Deng,

345   *Curr. Nanosci.*, 2013, 9, 8-13.

346   19.   H. B. Deng, X. Zhou, X. Y. Wang, C. Y. Zhang, B. Ding, Q. H. Zhang

347   and Y. M. Du, *Carbohydr. Polym.*, 2010, 80, 474-479.

348   20.   A. Shukla, J. C. Fang, S. Puranam, F. R. Jensen and P. T. Hammond,

349   *Adv. Mater.*, 2012, 24, 492-496.

350   21.   J. C. Antunes, C. L. Pereira, M. Molinos, F. Ferreira-da-Silva, M. Dessi,

351   A. Gloria, L. Ambrosio, R. M. Goncalves and M. A. Barbosa,

352   *Biomacromolecules*, 2011, 12, 4183-4195.

353   22.   P. Zhang, C. Shao, Z. Zhang, M. Zhang, J. Mu, Z. Guo and Y. Liu,

354   *Nanoscale*, 2011, 3, 3357-3363.

355   23.   X. Cao, B. Ding, J. Yu and S. S. Al-Deyab, *Carbohydr. Polym.*, 2012, 90,

356   1075-1080.

357   24.   J. Zhao, Z. Wei, X. Feng, M. Miao, L. Sun, S. Cao, L. Shi and J. Fang,

358   *ACS Appl. Mater. Interfaces*, 2014, DOI: 10.1021/am5026352.

359   25.   B. Zhou, Y. Hu, J. Li and B. Li, *Int. J. Biol. Macromol.*, 2014, 64,

360   402-408.

361   26.   T. Zhang, P. Zhou, Y. Zhan, X. Shi, J. Lin, Y. Du, X. Li and H. Deng,

362   *Carbohydr. Polym.*, 2015, 117, 687-693.

363   27.   Y. Zhan, W. Zeng, G. Jiang, Q. Wang, X. Shi, Z. Zhou, H. Deng and Y.

364   Du, *J. Appl. Polym. Sci.*, 2015, 132.

365   28.   D. S. Sheny, J. Mathew and D. Philip, *Spectrochim. Acta. A. Mol.*

366   *Biomol. Spectrosc.*, 2011, 79, 254-262.

367   29.   M. Meena Kumari, S. A. Aromal and D. Philip, *Spectrochim. Acta. A.*

368   *Mol. Biomol. Spectrosc.*, 2013, 103, 130-133.

369   30.   W. Li, X. Y. Li, W. Li, T. Wang, X. X. Li, S. Y. Pan and H. B. Deng, *Eur.*

370   *Polym. J.*, 2012, 48, 1846-1853.

371   31.   T. Zeng, X. Zhang, Y. Guo, H. Niu and Y. Cai, *J. Mater. Chem. A*, 2014,

372   2, 14807.

373   32.   N. Vasimalai and S. A. John, *J. Mater. Chem. A*, 2013, 1, 4475.

374   33.   B. Zhou, Y. Li, H. Deng, Y. Hu and B. Li, *Colloids Surf. B Biointerfaces*,

375   2014, 116C, 432-438.

376   34.   S. K. Maji, S. Sreejith, A. K. Mandal, X. Ma and Y. Zhao, *ACS Appl.*

377   *Mater. Interfaces*, 2014, DOI: 10.1021/am503110s.

378   35.   J. Zheng, Y. Dong, W. Wang, Y. Ma, J. Hu, X. Chen and X. Chen,

379   *Nanoscale*, 2013, DOI: 10.1039/C3NR01075A.

380   36.   L. Qiu, Y. Peng, B. Liu, B. Lin, Y. Peng, M. J. Malik and F. Yan, *Appl.*

381   *Catal. A-gen.*, 2012, 413-414, 230-237.

382

383

384

385

386

387

388

389

390

391

392

393

394

395

396

397   **Figure captions:**

398   **Figure 1.** Figure 1. SEM images of (a-d): cellulose nanofibrous mats, (Lys/TA)$_2$,

399   (Lys/TA)$_5$, and (Lys/TA)$_{10}$. Image (a'-d') showed high magnification images of

400   a-d, respectively. The right column reveals the diameter distribution

401   histograms of the nanofibrous mats.

402   **Figure 2.** FT-IR spectra of (a-e): Lys, TA, (Lys/TA)$_5$, (Lys/TA)$_{10}$, and cellulose

403   nanofibrous mats.

404   **Figure 3.** Figure 3. SEM images of (AuNPs@Lys/TA)$_{10}$ (a); high magnification

405   image (b).

406   **Figure 4.** Cross-sectional TEM images of AuNPs-immobilized nanofibers with

407   different magnification (reduced in 1mM HAuCl$_4$ solution) (a-c); the particle

408   size distribution histogram (d)

409   **Figure 5.** XPS survey speatra of (AuNPs@Lys/TA)$_{10}$ (a) and core-level spectra

410   of C 1s, N 1s, S 2p, and Au 3d (b-e); EDS speatra of (AuNPs@Lys/TA)$_{10}$ (f).

411   **Figure 6.** XRD patterns of cellulose nanofibrous mats (a), (AuNPs@Lys/TA)$_5$

412   (b), (AuNPs@Lys/TA)$_{10}$ (c).

413   **Figure 7.** Catalytic performance of composite nanofibrous mats. (a) At/A$_0$

414   *versus* reaction time for the reduction of 4-NP; (b) catalytic activity of the

415   (AuNPs@Lys/TA)$_5$ with three times of cycling uses.
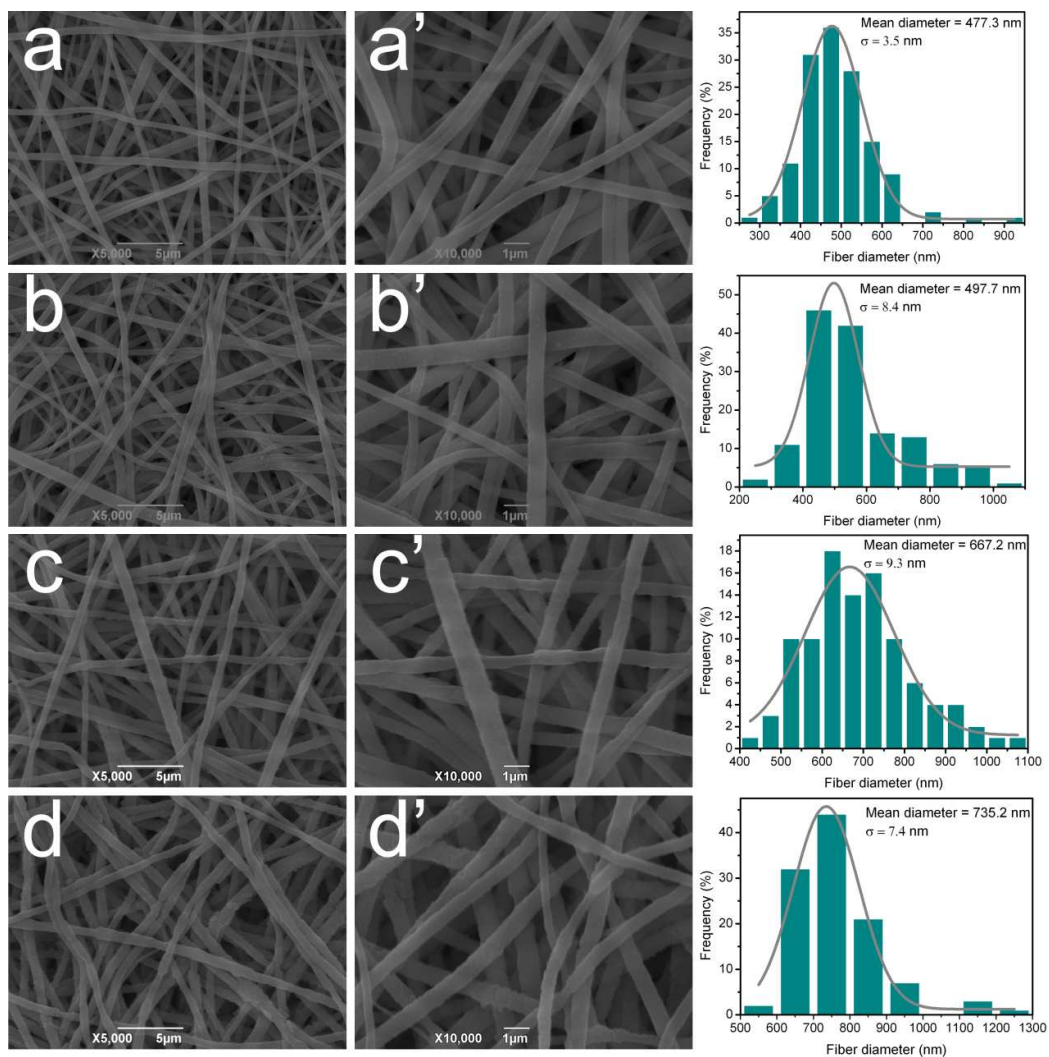
416

417

418

419

420   Figure 1
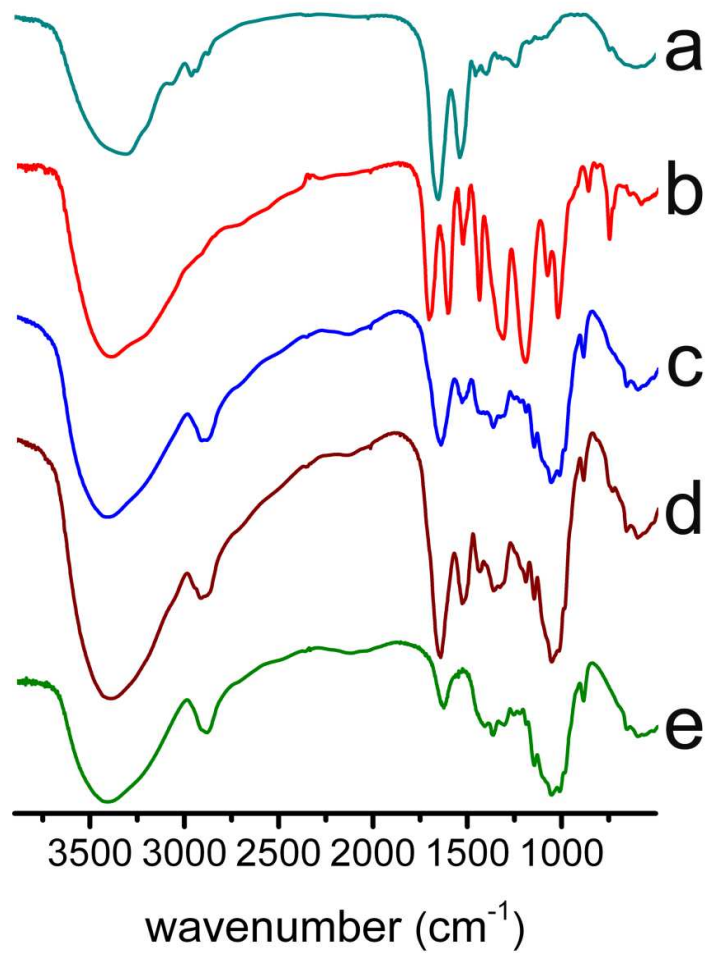

421
422
423
424
425
426
427
428

429

430 Figure 2

431
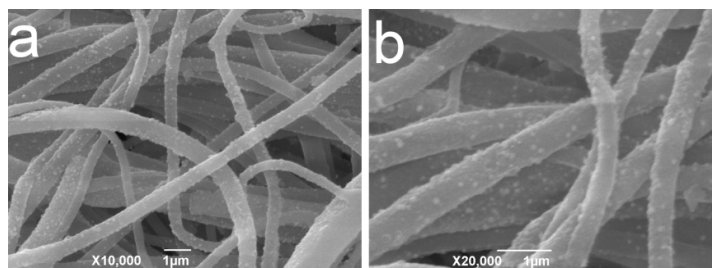432
433
434
435
436
437
438
439

440   Figure 3

441

442

443

444

445

446

447

448

449

450

451

452

453

454
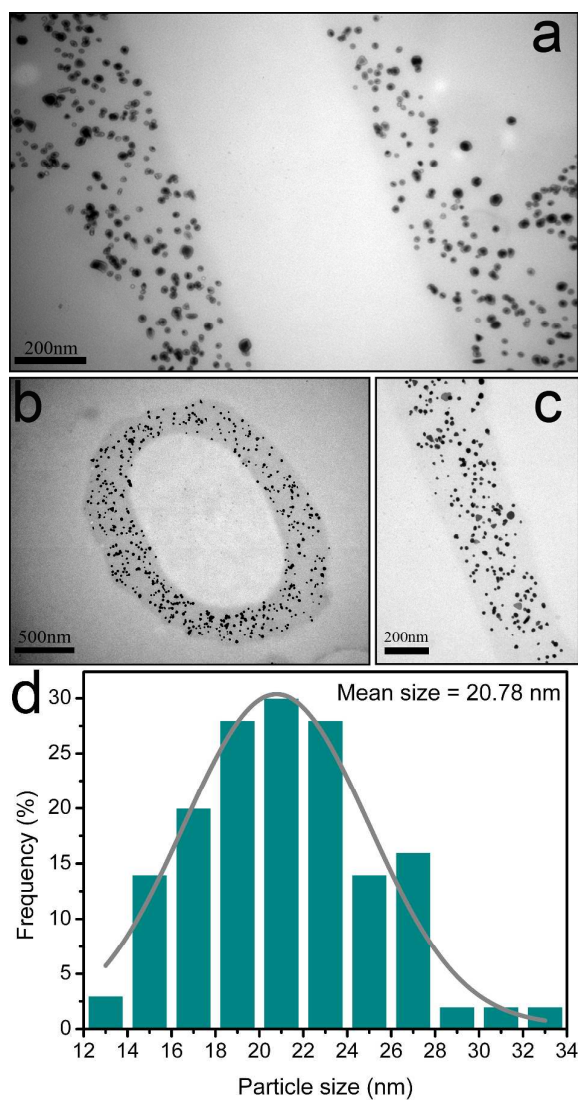
455

456

457

458

459

460   Figure 4

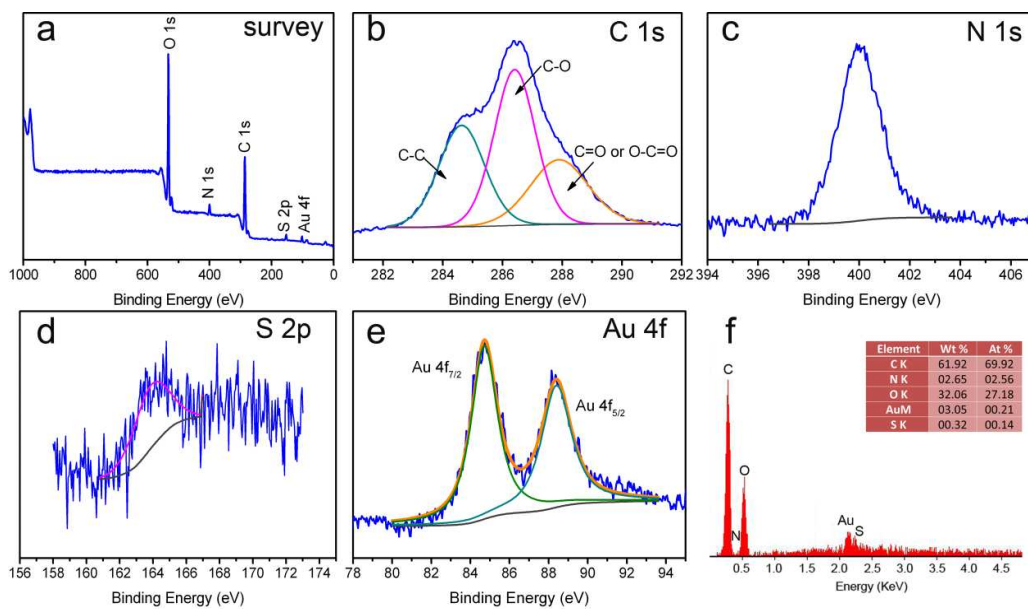461

462

463

464

465

466

467

468

469 Figure 5

470

471

472

473

474

475

476

477

478

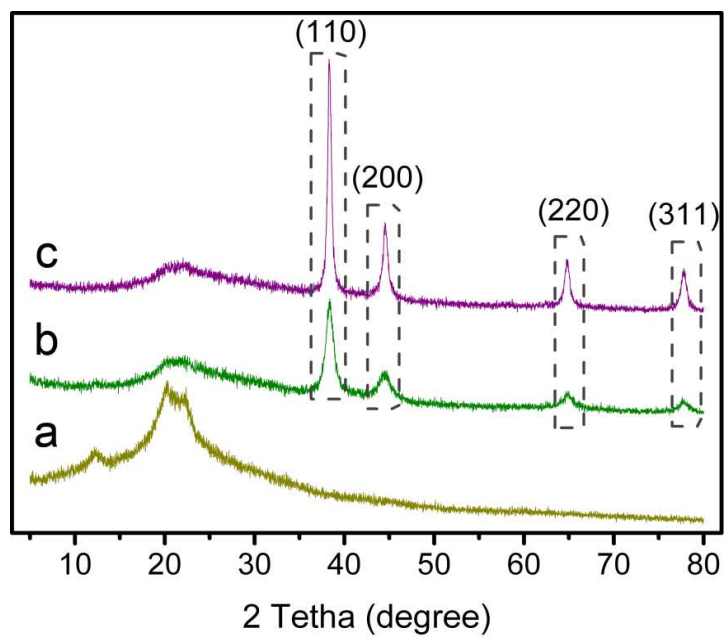479

480

481

482

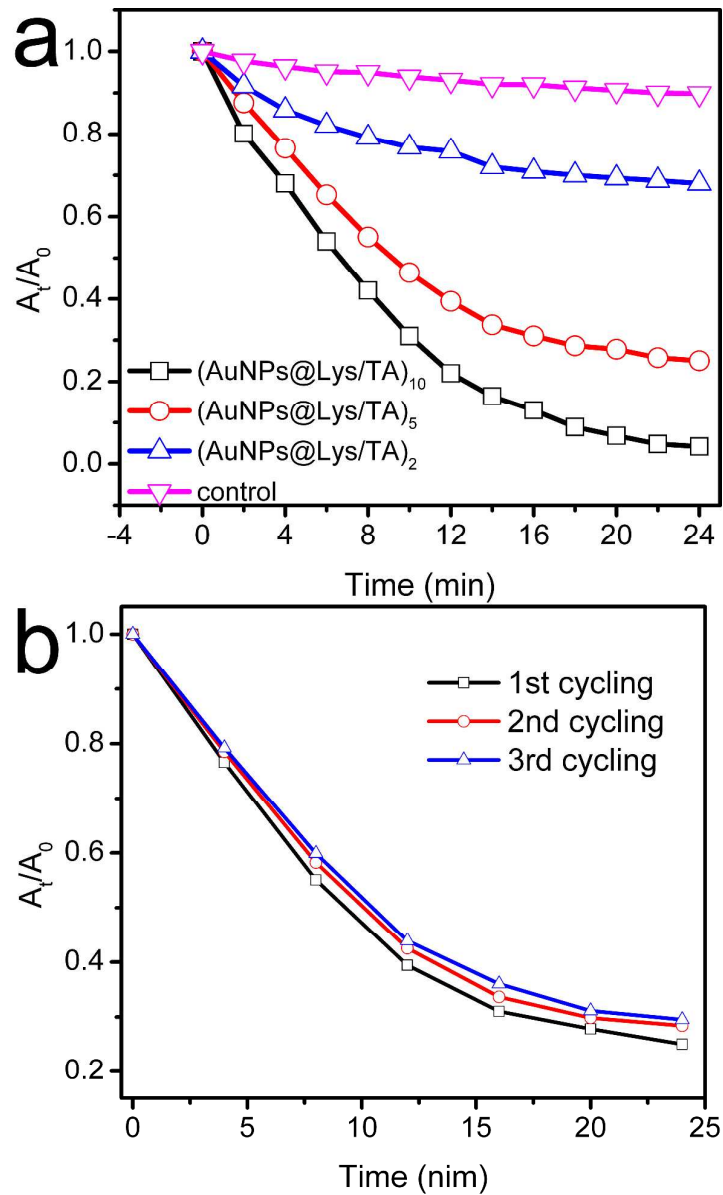483

484   Figure 6

485

486

487

488

489

490

491

492

493

494

495

496

497

498

499   Figure 7

500

501

502